Free energy and concentration of crystalline vacancies by molecular simulation

Apoorva Purohit, Andrew J. Schultz, Sabry G. Moustafa, Jeffrey R. Errington, and David A. Kofke*
Department of Chemical and Biological Engineering,
University at Buffalo, The State University of New York,
Buffalo, New York 14260-4200, USA
(Dated: May 3, 2018)

We present an approach for evaluating the concentration of vacancy defects in crystalline materials by molecular simulation. The proposed method circumvents the problem of equilibration of the number of "lattice sites" M, which characterizes the tradeoff between more, smaller lattice cells (with some vacant), versus fewer, larger cells. Working in a grand-canonical framework, we instead fix M and solve for the chemical potential μ that ensures thermodynamic consistency of the ensemble-averaged pressure and the grand potential. Having determined μ this way for the given M, the equilibrium vacancy concentration and free energy are easily determined. Methods are demonstrated for the classical Lennard-Jones fcc crystal, examining all states where the crystal is stable. We find for this system that the effect of equilibrating M is negligible at all conditions. Also, although the vacancy fraction varies by many orders of magnitude with temperature and density, we find that the value at melting is nearly independent of density, equal to about 2×10^{-4}. Results further show that a lattice-energy approximation (ignoring entropic effects) underestimates the correct concentration by four orders of magnitude at almost all conditions; ignoring only anharmonic contributions underestimates the vacancy concentration at melting by nearly one order of magnitude.

I. INTRODUCTION

Point defects are known to occur naturally in crystalline materials and have a disproportionate impact on their properties and performance. Point defects are thermodynamically stable, so they are present in fully equilibrated crystals. Both experimental and computational studies have been conducted in order to estimate their behavior [1]. A difficulty facing experimental studies is the presence of a wide variety of point defects along with extended defects such as dislocations and grain boundaries, which makes it difficult to separate the effects of these different defects and their interactions [2, 3]. Consequently some uncertainty in the interpretation of the experimental results remains and hence, computational studies are required.

Two issues complicate the study of point defects via molecular modeling. First, the formalism for treatment of point defects, and vacancies in particular, is clouded by a subtlety in accounting for how free volume is distributed—in particular whether it should be allocated to occupied sites to give each particle more freedom to move, or whether it should be used to make more vacancies [4, 5]. Second, as an equilibrium property, defect behavior is understood through reference to the free energy (FE), and free energies in general are problematic to evaluate by molecular simulation [6–8].

The first issue is illustrated in Fig. 1. Each large box in the figure describes the nominal arrangement of the atoms during the simulation of a crystal. The filled cells in the boxes describe the regions sampled by each of the individual atoms, one atom per filled cell. The atoms are not constrained to sample the cells; rather the implication is that this is where they sample naturally when equilibrated. In this simple example the atoms arrange themselves on a cubic lattice. The case on the left of the figure has no defects, and the number of cells (or lattice sites) M equals the number of atoms N (400 in the example). In the arrangement on the right, the system has more but slightly smaller cells, $M = 441$, but the same N, so the excess lattice sites represent vacancy defects (depicted by the non-filled cells).

The complication is that the canonical ensemble comprises both of these arrangements (and many more), and to properly sample the ensemble it must be possible to consider all such cases. However, a conventional NVT simulation (where V is the volume, and T the temperature) of a feasible sampling length is not able to make the concerted moves needed to reach one arrangement from the other — the simulation is non-ergodic in this respect. Even worse, a finite-size system may not be able to accommodate the values of M that are representative of the equilibrated system. This is illustrated with the red boxes, which represent simulations of smaller systems. We see that the zero-defect arrangement can be accommodated in this smaller volume, but the system having the cells on the right cannot.

One manifestation of this problem is that the usual grand-canonical FE does not vary in proportion to the volume, which means, for example, that a plot of pressure P versus chemical potential μ at fixed T (and M) will not be independent of V, as it would be for a fluid (see Appendix A for an example). In a sense, M represents another extensive parameter that is in play. Accordingly, the issue is sometimes treated or described as if the lattice sites were real physical quantities, akin to molecules, with an effective chemical potential [4]. This is

* kofke@buffalo.edu

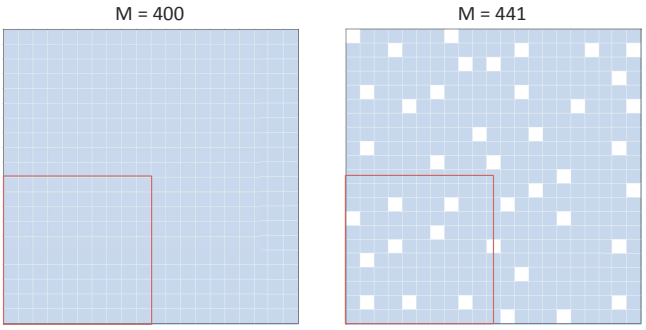

FIG. 1: Illustration of the problem. Both systems have the same number of atoms N (represented by filled cells) and total area, but different numbers of lattice sites M (left is 20×20, right is 21×21).

a valid description, but one should be careful not to take the interpretation too far. The lattice sites are not physically real in the sense that they are not conserved, and there is no direct reason for them to equilibrate across two phases, for example. Instead, one could view M as an order parameter, characterizing partitions of phase space. To the extent that the system is able to equilibrate across these regions, M represents an unconstrained degree of freedom, and it will take a value that minimises the FE within the constraints of the governing ensemble.

Both Swope-Andersen [4] and Pronk-Frenkel [5] give a prescription for determining the equilibrium M value ($M_{\rm eq}$) in order to evaluate the crystalline properties and vacancy concentration correctly, although neither demonstrate in an application. Reference [4] prescribes a method that is essentially equivalent to searching over V/M and N/M to find conditions such that the thermodynamic Euler equation is satisfied. Reference [5] works within the grand-canonical ensemble, and describes a method for $M_{\rm eq}$ based on expanding the FE in terms of M, requiring measurement of the compressibility. We have formulated an alternative to these approaches, which appears to be much simpler to implement. This is described in Sec. II.

Turning now the problem of evaluating the relevant FE, a large portion of the computational studies considers only the zero-temperature defect energies [9]. These are computed by molecular statics or energy minimization techniques. However, the behavior predicted using zero-Kelvin lattice energies might not be valid at higher temperatures, as the harmonic and anharmonic contributions are neglected. Another approach widely used is to employ the defect formation energies (not free energies) at non-zero temperatures calculated by ensemble averaging using molecular simulation techniques [10, 11]. However, at higher temperatures, the entropic contributions become significant, which are completely neglected via this approach.

Harmonic methods (quasiharmonic and local harmonic) have been used for computing the FE for the formation of defects [12–14] while accounting for entropic contributions. These methods are based upon the assumption that atoms vibrate within quadratic potential wells and thus, the full Hamiltonian can be replaced by a harmonic expansion about the equilibrium positions [15, 16]. However, the harmonic methods are known to break down at temperatures above roughly half of the melting point in case of solids containing point defects [17], and in such circumstances, techniques that can also include the anharmonic contributions are needed. One such technique is thermodynamic integration (TI), which is widely used to calculate the FE for the formation of defects [18–20]. However, the limitation of this method is that in order to obtain adequate statistical accuracy for the determination of excess thermodynamic properties at a defect, a large number of molecular simulation steps are required, thereby demanding substantial computational resources. This is a particularly acute problem when employing ab initio potentials, such as density functional theory (DFT) to model the interatomic interactions. Some earlier works have also reported the problem of large error bars while calculating the vacancy formation FE using the TI method [13, 17]. Thus, there is a clear need for FE methods that can improve the accuracy for crystalline systems with defects.

In this regard, we recently proposed the harmonically mapped averaging (HMA) method for evaluation of crystalline properties via molecular simulation [21]. In this method, the analytically known harmonic behavior of the crystal is removed from the traditional ensemble averages, which leads to an accurate and precise measurement of the anharmonic contributions without contamination by noise produced by the already-known harmonic behavior. Thus, the HMA method improves precision in the anharmonic contributions to the extent that harmonic behavior contributes to the noise in molecular simulation. In case of defect-free crystals, it has proved to be much more efficient than the conventionally used TI method [21]. In this paper, we examine the efficiency and range of validity of the HMA method for calculating the free energies of point defects in crystals.

An alternative to TI for evaluation of vacancy FE involves particle insertions and deletions. With appropriate biasing methods, such an approach can be very effective, particularly for simple monatomic molecules. We examine such methods in the present work as well.

The outline of this paper is as follows. In the next section, we describe the new formalism for calculating the properties of vacancy defects at finite temperature. Sec. III describes the FE methods we use in this study, while Sec. IV presents the simulation details. Sec. V presents the results obtained using the three FE methods in our formalism, and the last section provides a summary as well as the conclusions.

II. FORMALISM

A. Grand-canonical ensemble

The grand-canonical partition function Ξ can be written as a sum over the number of vacancies n:

$$\Xi(T,V,\lambda;M) = \mathrm{e}^{-\beta L} = \sum_{n=0}^{n_{\max}} \lambda^{M-n}\mathrm{e}^{-\beta A_n} \tag{1}$$

where L is the grand-canonical potential, defined in terms of the activity $\lambda \equiv \exp(\beta\mu)$ with μ the chemical potential, and $A_n \equiv A(T,V,M-n;M)$ is the Helmholtz FE of the system with n vacancies; also $\beta = 1/k_\mathrm{B}T$ with k_B Boltzmann's constant, and $n_{\max}$ is some practical upper limit to the number of vacancies, typically set such that contributions from $n > n_{\max}$ are negligible. Equation (1) assumes that interstitials ($n < 0$) are not relevant to behavior. Alternatively,

$$\mathrm{e}^{-\beta L} = \lambda^M \mathrm{e}^{-\beta A_0} \sum_{n=0}^{n_{\max}} \lambda^{-n}\mathrm{e}^{-\beta\Delta A_n} \tag{2}$$

where $\Delta A_n \equiv A_n - A_0$.

We can also write the probability of having n vacancies,

$$\begin{aligned} p_n &= \mathrm{e}^{+\beta L}\lambda^{M-n}\mathrm{e}^{-\beta A_n} \\ &= \frac{\lambda^{-n}\mathrm{e}^{-\beta\Delta A_n}}{\sum_{n=0}^{n_{\max}}\lambda^{-n}\mathrm{e}^{-\beta\Delta A_n}}. \end{aligned} \tag{3}$$

The pressure in the grand-canonical ensemble uses this weighting in an average over the number of possible vacancies:

$$\bar{P}(T,V,\lambda;M) = \sum_{n=0}^{n_{\max}} P_n p_n, \tag{4}$$

where P_n is the pressure for the system with n vacancies.

The Euler equation for this ensemble is simply

$$L = -\bar{P}V. \tag{5}$$

Given values for A_0 and ΔA_n for relevant n (typically $n = 1$ is enough), we handle the determination of M_eq by satisfying (5). However, we do not attempt to solve for M_eq for given V and λ, rather we perform the much easier task of solving for λ satisfying (5) for the given V and M. For this value of λ, the M for which we collected our data will be M_eq. Having determined λ this way, we can evaluate the equilibrium fraction of vacancies, ϕ, via:

$$\phi \equiv \frac{\bar{n}}{M} = \frac{M-\bar{N}}{M} = \frac{1}{M}\sum_{n=0}^{n_{\max}} n p_n \tag{6}$$

It is worth noting that the framework described above does not allow for variation of M in the sum over vacancies that defines Ξ. The true grand partition function includes fluctuations in M, but we show in Appendix B that this effect contributes $\mathcal{O}(\ln M)$ to the (extensive) FE L, and hence it may be treated as a finite-size effect.

B. Intensive properties and thermodynamic derivatives

The discussion above has emphasised that in a physically correct treatment of lattice systems, M is a dependent quantity. Accordingly, thermodynamic properties are naturally expressed in terms of FE derivatives that do not constrain M, and to relate properties to the FE we should work with data in which M varies freely as the state is changed. However, simulation data are much simpler to collect while holding M fixed, and the framework developed above gives us a means to proceed this way. In this section we relate FE derivatives for fixed M to the conventional FE derivatives so that we can more easily connect our constant-M simulation data to the FE.

It is convenient and instructive to work with intensive quantities, formed by dividing by N, which we represent with lower-case variables that correspond to their upper-case extensive counterparts (e.g., $v \equiv V/N$). Further, we affix a tilde on variables that are made intensive by division by M (e.g., $\tilde{v} \equiv V/M$). For a property X, the two forms are related as

$$\tilde{x} \;=\; (1-\phi)x$$

Thus, the molar Helmholtz FE is $a = a(T,v;\phi)$. In this representation, the vacancy fraction ϕ (acting in lieu of M) adopts a value to minimise the FE in the equilibrated system. In terms of the intensive variables, the equilibrated state for a system simulated at given (T, $\tilde{v}$) is determined by solving for λ in

$$\ln\lambda + \frac{1}{M}\ln\sum_{n=0}^{n_{\max}}\lambda^{-n}\mathrm{e}^{-\beta\Delta A_n} = \beta\tilde{a}_0 + \bar{P}(\lambda)\tilde{v} \tag{7}$$

Assuming proper equilibration of ϕ, the Helmholtz FE of the crystal obeys the usual relations for a pure-component system. In particular, the pressure, molar energy, and chemical potential are

$$P = -\left(\frac{\partial a}{\partial v}\right)_T \tag{8a}$$

$$u = \left(\frac{\partial \beta a}{\partial \beta}\right)_v \tag{8b}$$

$$\mu = a + Pv \tag{8c}$$

We seek relations that reflect our control of $\tilde{v}$ rather than v. Manipulation of the corresponding derivatives yields the following expressions. First, the pressure:

$$P = -\left(\frac{\partial a}{\partial \tilde{v}}\right)_T \Big/ \left(\frac{\partial v}{\partial \tilde{v}}\right)_T \tag{9a}$$

with

$$\left(\frac{\partial v}{\partial \tilde{v}}\right)_T = \frac{1}{1-\phi} + \frac{\tilde{v}}{(1-\phi)^2}\left(\frac{\partial \phi}{\partial \tilde{v}}\right)_T \tag{9b}$$

The molar energy is a bit more complicated because we are changing not the differentiation variable, but the quantity held fixed during the differentiation:

$$\begin{aligned} u &= \left(\frac{\partial \beta a}{\partial \beta}\right)_{\tilde{v}} + \left(\frac{\partial \beta a}{\partial \tilde{v}}\right)_{\beta}\left(\frac{\partial \tilde{v}}{\partial \beta}\right)_{v} \\ &= \left(\frac{\partial \beta a}{\partial \beta}\right)_{\tilde{v}} + \frac{\beta P \tilde{v}}{(1-\phi)^2}\left(\frac{\partial \phi}{\partial \beta}\right)_{\tilde{v}} \end{aligned} \tag{10}$$

which uses (9a).

C. Relation to defect-free properties

Characterization of the defect-free lattice is the starting point for analysis of the lattice with vacancies, and it may be expected that the thermodynamic properties of the lattice with defects will be relatively small perturbations on the properties for the defect-free lattice. Therefore, analysis of simulation data is best done by considering separately the behavior of the defect-free system, and the perturbations resulting from the vacancies. Accordingly, we separate the Helmholtz FE:

$$a(T, v; \phi_{\mathrm{eq}}) = a_0 + \Delta a \tag{11}$$

where again $a_0 = a(T, V; \phi = 0)$, and can be evaluated via thermodynamic integration of data from simulation of the defect-free lattice; note that $a_0 = \tilde{a}_0$.

To evaluate Δa directly, we can manipulate Eq. (2). First we write it in intensive variables,

$$\beta l = -\frac{M}{N}\left(\ln\lambda - \beta a_0\right) - \frac{1}{N}\ln\sum_{n=0}^{n_{\max}} \lambda^{-n}\mathrm{e}^{-\beta\Delta A_n} \tag{12}$$

We can combine this with the definition of L as the Legendre transform of A, expressed here as:

$$l = a - \mu,$$

and an Euler relation, which is applicable because we are concerned with the M-equilibrated system:

$$k_{\mathrm{B}}T\ln\lambda \equiv \mu = a + Pv,$$

to yield

$$\beta\Delta a = -\frac{\phi}{1-\phi}\beta(Pv + \Delta a) - \frac{1}{N}\ln\sum_{n=0}^{n_{\max}} \lambda^{-n}\mathrm{e}^{-\beta\Delta A_n}$$

or

$$\beta\Delta a = -\frac{\phi}{1-\phi}\beta P\tilde{v} - \frac{1}{M}\ln\sum_{n=0}^{n_{\max}} \lambda^{-n}\mathrm{e}^{-\beta\Delta A_n} \tag{13}$$

Both terms on the right-hand side will be small for low vacancy concentrations, so this expression should yield a result for Δa with better precision than one based on (11), which involves the small difference between relatively large numbers.

The defect-free FE allows for no variation of ϕ, so its derivatives give the defect-free pressure P_0 and molar energy u_0. Substituting for a as given by (11), the volume and temperature FE derivatives become:

$$P = \left[P_0 - \left(\frac{\partial \Delta a}{\partial \tilde{v}}\right)_T\right] \Big/ \left(\frac{\partial v}{\partial \tilde{v}}\right)_T \tag{14}$$

and

$$u = u_0 + \left(\frac{\partial \beta \Delta a}{\partial \beta}\right)_{\tilde{v}} + \frac{\beta P\tilde{v}}{(1-\phi)^2}\left(\frac{\partial \phi}{\partial \beta}\right)_{\tilde{v}} \tag{15}$$

D. Case of noninteracting vacancies

The vacancy concentration in crystalline systems is usually very small, hence the assumption that vacancies do not interact can represent a reasonable approximation. The Helmholtz FE of a system with n noninteracting vacancies and M lattice sites is given by,

$$\mathrm{e}^{-\beta\Delta A_n} = \binom{M}{n}\mathrm{e}^{-\beta n\Delta A_1^{\mathrm{r}}} \tag{16}$$

where the residual FE difference ΔA_1^{r} is the change in the FE due to a single vacancy at a *specific location*, and the combinatorial multiplier accounts for the different ways of arranging the n vacancies among the M lattice sites.

With this form, the summation for Ξ in Eq. (1) is just a binomial expansion (if we take $n_{\max} = M$), and can be summed to yield:

$$L(T, V, \mu; M) = A_0 - Mk_{\mathrm{B}}T\ln\left(\lambda + e^{-\beta\Delta A_1^{\mathrm{r}}}\right). \tag{17}$$

The average N can then be obtained using:

$$\bar{N} = -\beta\lambda\left(\frac{\partial L}{\partial \lambda}\right)_{T,V} = M\frac{\lambda}{\lambda + e^{-\beta\Delta A_1^{\mathrm{r}}}}, \tag{18}$$

and from this, the vacancy concentration is:

$$\phi = \frac{e^{-\beta\Delta A_1^{\mathrm{r}}}}{\lambda + e^{-\beta\Delta A_1^{\mathrm{r}}}}. \tag{19}$$

Given Eq. (17), the pressure can be expressed:

$$\bar{P} = -\left(\frac{\partial L}{\partial V}\right)_{T,\lambda} = P_0 + M\phi\Delta P_1. \tag{20}$$

Upon application of Eq. (5) to determine the value of λ that yields M at equilibrium, we can use Eq. (19) to eliminate λ to obtain directly an expression for the vacancy concentration:

$$-k_{\mathrm{B}}T\ln\phi = \tilde{a}_0 + P_0\tilde{v} + \Delta A_1^{\mathrm{r}} + \Delta P_1\tilde{v}M\phi. \tag{21}$$

We note that $\tilde{a}_0 + P_0\tilde{v}$ is the chemical potential of the defect-free system. Given measurements for this quantity, and the vacancy-formation values ΔA_1^{r}, ΔP_1, this equation can be solved numerically for ϕ.

It is instructive to examine the relatively simple formulas for noninteracting vacancies, comparing the M-equilibrated result, (21), with the corresponding equation obtained when M is not equilibrated [5]:

$$-k_{\rm B}T\ln\phi = \tilde{a}_0 + P_0\tilde{v} + \Delta A_1^{\rm r}. \tag{22}$$

The difference between these formulas is just the last term in Eq. (21), which is $\mathcal{O}(\phi)$ and will often be small in comparison to the $\mathcal{O}(1)$ terms that make up the rest of the equation. This suggests that the effect on ϕ of equilibrating M will be small, unless there is a high concentration of vacancies. Increasing ϕ also leads to more significant interactions between vacancies, which can further act to affect the importance of M-equilibration.

III. EVALUATION OF ΔA_n

The key input needed in the framework outlined above is the FE for formation of n vacancies, ΔA_n. This is evaluated by molecular simulation. We describe here two approaches that might be used for this purpose.

A. Thermodynamic Integration (TI)

According to the TI technique, the change in Helmholtz FE of a system from initial temperature T_0 to a final temperature T can be evaluated as follows [22]:

$$\frac{A(T)}{k_BT} = \frac{A(T_0)}{k_BT_0} - \int_{T_0}^{T}\frac{U(T')}{k_BT'^2}dT'. \tag{23}$$

where $U(T')$ denotes the configurational energy at an intermediate temperature T' between T_0 and T, such that the integration is performed along a reversible path connecting both the states. When integrating from a very low temperature (i.e. $T_0 \to 0$), the $1/T_0^2$ and $1/T_0$ divergences of Eq. (23) can be removed by separating the Helmholtz FE into lattice-energy, harmonic, and anharmonic contributions [23, 24]:

$$A(T) = U^{\rm lat} + A^{\rm qh}(T) + A^{\rm ah}(T). \tag{24}$$

The first term represents the configurational lattice energy ($U^{\rm lat}$), calculated by energy minimization with respect to the atom positions. The next term ($A^{\rm qh}$) represents the harmonic contribution to the FE, calculated via [17, 25]:

$$\beta A^{\rm qh}(T) = \frac{1}{2}\sum_{j=1}^{3N-3}\ln\frac{\lambda_j}{2\pi k_BT} - \frac{3}{2}\ln N - \ln v \tag{25}$$

where λ_j are the non-zero eigenvalues of the $(3N\times 3N)$ Hessian matrix of the minimized potential energy, as described in the literature [16]. The third term ($A^{\rm ah}$) represents the anharmonic contribution to the FE, calculated via [21]:

$$A^{\rm ah}(T) = -T\int_0^T\frac{U^{\rm ah}(T')}{T'^2}dT'. \tag{26}$$

where $U^{\rm ah}(T')$ represents the anharmonic configurational energy at a temperature T'.

The vacancy-formation FE $\Delta A_{\rm n}$ is calculated by differencing the TI-computed free energies of systems of n and zero vacancies, respectively. In principle, a separate integration is needed for each n, and for $n>1$ it is necessary to sample locations of the vacancies in the lattice. We do not pursue this approach, and instead rely on the independent-vacancy approximation (Sec. II D), evaluating the FE of formation of only a single vacancy. The difference gives the residual FE defined in Eq. (16):

$$\Delta A_1^{\rm r} = \Delta U^{\rm lat} + \Delta A^{\rm qh} + \Delta A^{\rm ah}. \tag{27}$$

The two methods that were used in calculating the anharmonic configurational energy are described below: (1) the conventional averaging technique (referred to as conventional TI in this paper) and the recently developed (2) harmonically-mapped averaging technique (referred to as HMA in this paper).

1. *Conventional averaging*

The traditionally used ensemble averaging technique is based on the direct calculation of ensemble average of the total configurational energy using molecular simulation. Thus, the anharmonic configurational energy is obtained by subtracting the harmonic and lattice energy contributions from the ensemble-averaged total configurational energy as follows:

$$U^{\rm ah} = \langle U\rangle - U^{\rm lat} - U^{\rm qh}, \tag{28a}$$

$$U^{\rm qh} = \frac{3}{2}(N-1)k_BT. \tag{28b}$$

2. *Harmonically-mapped averaging (HMA)*

The conventional ensemble averaging technique does not exploit the known harmonic character of crystalline systems; rather, the harmonic contributions to properties are computed stochastically via molecular simulation, and consequently ensemble averages suffer from the uncertainty that these contributions introduce. This problem is circumvented when using HMA, which yields directly the anharmonic contribution to the energy. The details of this method can be seen in our previous work [21]. One of the important applications of the HMA method is evaluation of FE of crystalline systems using

the TI technique, where the reformulated ensemble average of the total configurational energy (in case of canonical ensemble) is given by [21]:

$$\langle U\rangle_{\rm HMA} = \frac{3}{2}(N-1)k_BT + \left\langle U + \frac{1}{2}\mathbf{F}\cdot\Delta\mathbf{r}\right\rangle, \quad (29)$$

where $\mathbf{F}$ is the vector (of length $3N$) of forces on each atom in the simulation box, and $\Delta\mathbf{r}$ is the corresponding vector of displacements of the atoms from their respective lattice sites. For a harmonic system, $-\mathbf{F}\cdot\Delta\mathbf{r}/2$ is exactly equal to the total energy (beyond $U^{\rm lat}$), so the harmonically-mapped average of $\langle U + \mathbf{F}\cdot\Delta\mathbf{r}/2\rangle$ is exactly equal to $U^{\rm lat}$ if applied to a harmonic system. Added to this average is the analytic expression for the harmonic configurational energy of the crystalline system (i.e. $3k_BT(N-1)/2$). Therefore, the anharmonic configurational energy contribution is directly measured by subtracting the lattice energy from the harmonically-mapped average as shown in Eq. (30).

$$U^{\rm ah} = \left\langle U + \frac{1}{2}\mathbf{F}\cdot\Delta\mathbf{r}\right\rangle - U^{\rm lat}. \quad (30)$$

This form of the average may then be used when evaluating the integral in Eq. (26).

The effectiveness of HMA relies on identifying an appropriate lattice site for each atom, about which its position fluctuates. The presence of a vacancy can promote the diffusion of atoms, causing them to fluctuate about sites that are different from the ones they were assigned at the start of the simulation. The computed averages do not in principle lose accuracy in such a circumstance, but the precision advantage is compromised. Various remedies can be conceived to address this problem: one can impose constraints that prevent diffusion events, but perhaps introducing inaccuracy in the computed free energy; alternatively one can track atom locations and move the designated lattice site of an atom if it diffuses.

Diffusion events are less likely at lower temperature and higher density, which are also the conditions where HMA is most effective relative to conventional averaging. In the present study we did not attempt to artificially prevent or compensate for the effect of diffusion on HMA averaging. Rather we discarded any HMA results for simulations where any diffusion event was observed, and replaced it with the conventional average, which was evaluated in the same simulation run. In multiple independent runs at a given state, we sometimes observed diffusion in some but not others, and in such cases we generated results by combining HMA averages from diffusion-free runs with conventional averages from diffusion-observed simulations, weighted to minimize the uncertainty in the overall average.

B. Grand-canonical Sampling

An alternative to TI for evaluating ΔA_n is to perform sampling of the number of vacancies n, simulating in the grand-canonical ensemble. The molecule insertions and deletions prescribed by this ensemble will not be very efficient if performed in the conventional way; most trials will be rejected because insertion in the high-density crystal will often result in high-energy overlaps that are rejected, while deletions will be proportionally rejected due to the high chemical potential that discourages particle removals. Biasing methods have been developed to overcome these difficulties [26], but they attempt to insert at/near unoccupied cells. The approach that we have employed here, exploits the local crystalline structure of the solids for insertion.

In the following sections, we detail the methods we use for biasing trials so that they lead to reasonable acceptance rates, and biasing sampling so that we explore an appropriate range of vacancy numbers. We also describe how we compute the needed FE differences ΔA_n from our simulation data.

1. Trial bias

We can improve sampling by attempting to insert atoms at positions that have a high probability of being a vacancy, identifying such positions by inserting next to an existing atom that does not have enough nearest neighbors. For an fcc lattice, we start the process of insertion by identifying all atoms that have fewer than 12 nearest neighbors (atoms whose distance is less than $r_{\rm nbr}$). We choose one atom from the list of these candidates at random. We then choose one of 12 lattice vector offsets to give an insertion site. The new atom is inserted at a position chosen randomly from within a sphere of radius $r_{\rm max}$ around the insertion site. The probability of accepting the insertion is a function of the energy change due to insertion, but also on the probability of choosing the newly-inserted atom for deletion.

For deletion, we identify candidates for deletion as an atom at a position which could be chosen as an insertion position if the atom were not present. To do this, we find all atoms (atom 1) that have 12 or fewer nearest neighbors. For each neighbor (atom 2) of those atoms, we consider it to be a candidate for deletion if it is within $r_{\rm max}$ of a lattice offset from atom 1. If an atom satisfies the criteria multiple times (if there are multiple atoms with 12 or fewer nearest neighbors that include the candidate as a neighbor), then the candidate is chosen in proportion to the number of times it satisfies the criteria. The probability of accepting the deletion is a function of the energy of the deleted atom, but depends also on the probability of inserting an atom at the deleted site.

Having defined how we conduct insertion and deletion trials, we can write expressions for the probability of accepting these attempts. The probabilities for accepting the insertion or deletion of an atom following the trial

protocols described above are

$$P_{N\to N+1} = \min(1,\chi) \tag{31a}$$
$$P_{N+1\to N} = \min(1,1/\chi) \tag{31b}$$

with

$$\chi = \frac{12 n_{\rm ic} v_{\rm shell}}{n_{\rm dc}} e^{-\beta u_i} \tag{31c}$$

where $v_{\rm shell} = \frac{4\pi}{3} r_{\rm max}^3$, $n_{\rm ic}$ is the number of candidates for insertion (those atoms with fewer than 12 nearest neighbors) for the system of N atoms, and $n_{\rm dc}$ is the number of candidates for deletion (atoms which satisfy the criteria multiple times are counted as many times as they satisfy the criteria) for the system of $N+1$ atoms.

2. Sampling bias

The biased trials of the grand-canonical sampling scheme are corrected at acceptance, and consequently the method samples the appropriate number of vacancies for the system conditions. This outcome is not necessarily desired, because systems at low temperature may never sample a configuration with a vacancy, while large systems near the melting point may rarely sample a configuration without a vacancy. This is a problem because to connect to the defect-free system that forms the basis of our analysis method, we require information about the system for all values of n from $n = 0$ to some value beyond $\bar{n}$. To achieve this, we bias, or artificially weight, the sampling of the vacancy number n, and we remove the bias by appropriately re-weighting the averages.

To formulate the bias, we take an initial estimate of the single-vacancy FE, $\Delta A_1^{\rm r}$ and use the noninteracting-vacancy approximation (Sec. II D) to generate an estimate $p_n^{\rm non}$ of the probability for observing n vacancies. Combining Eqs. (3) and (16),

$$p_n^{\rm non} \propto \binom{M}{n} \left(\lambda e^{-\beta \Delta A_1^{\rm r}}\right)^n . \tag{32}$$

Let $n_{\rm m}$ be the n where this p_n has a maximum. Then, for $n < n_{\rm m}$ we weight sampling to nominally yield equal probability of visiting all $n < n_{\rm m}$, while for $n > n_{\rm m}$ we enhance sampling additional vacancies but attenuate the bias to limit the largest n sampled. Specifically, we define the weight w_n such that:

$$\frac{w_{n+1}}{w_n} = \begin{cases} p_n^{\rm non}/p_{n+1}^{\rm non} & n \le n_m \\ \min\left[1, 2p_n^{\rm non}/p_{n+1}^{\rm non}\right] & n > n_m \end{cases} \tag{33}$$

Trials are performed as already described, and acceptance is based on a reweighting of the χ defined in Eq. (31c):

$$\chi^{\rm bias} = \frac{w_{n+1}}{w_n}\chi \tag{34}$$

3. Computing Vacancy Free Energies

The vacancy free energies are computed as a part of performing Monte Carlo (MC) moves. When a move is attempted, the value of χ (as given by Eq. (31c)) is collected and used within a Bennett acceptance ratio scheme[27]:

$$X_{n,n+1} = \left\langle \frac{1}{1+\alpha/\chi} \right\rangle$$
$$X_{n+1,n} = \left\langle \frac{1}{\alpha+1/\chi} \right\rangle \tag{35}$$

where α is based on an estimate of the FE ($\alpha = \exp(-\beta(A_{n+1} - A_n))$) and the first formula is used for insertion and the second formula used for deletion. Then the FE itself can be computed as

$$\beta(A_{n+1} - A_n) = -\ln \frac{X_{n,n+1}}{X_{n+1,n}} \tag{36}$$

In principle, the FE difference is itself needed to compute the FE difference, but in practice the computed result is not very sensitive to α so long as it is reasonably close. Accordingly, we take an estimate of the FE difference from preliminary simulations and then use 11 values of α (same for all n) to collect data during the simulation. The α values are uniformly distributed on a logarithmic scale from $\alpha_0 e^{-6}$ to $\alpha_0 e^{+6}$ where α_0 is the estimate based on preliminary simulations.

IV. SIMULATION DETAILS

We employed the Lennard-Jones (LJ) model defined by the pair potential: $U(r) = 4\epsilon_{\rm LJ}((\sigma_{\rm LJ}/r)^{12} - (\sigma_{\rm LJ}/r)^6)$, where $\sigma_{\rm LJ}$ and $\epsilon_{\rm LJ}$ are the LJ size and energy parameters, respectively, and r is the pair separation. The LJ potential was truncated and shifted at $r_c = 4\tilde{v}^{-1/3}$, and $\sigma_{\rm LJ}$ and $\epsilon_{\rm LJ}/k_{\rm B}$ parameters were set to unity (LJ units). The system energy was corrected by adding the difference in lattice energies with and without the shift (equal to number of interacting lattice neighbors multiplied by the shift), but this correction was adjusted when vacancies were present. With n vacancies, the correction was taken to be $(U_{\rm noshift} - U_{\rm shift})(M-2n)/M$. Periodic boundary conditions were employed in all three orthogonal directions.

All simulations were performed with the Etomica simulation package [28] at conditions that encompass the region of stability of the LJ fcc crystal system [29–33]. To better represent the full range of behavior, we employ the following state variables in lieu of the temperature and density: a density-scaled temperature, $Y \equiv T\tilde{v}^4/4$, and the square of the molar volume, $\tilde{v}^2$ (as indicated by the tilde, in principle the volume reduced by M is what

we control to specify the state). The parameter Y in particular is useful for the LJ model, as it remains finite and meaningful in the soft-sphere limit, which is obtained as $\tilde{v}^2 \to 0$, and it is always less than about 0.5 for all stable crystalline states. Further, we observe that properties vary more uniformly with respect to $\tilde{v}^2$ rather than $\tilde{v}$ itself, so we take this as the independent variable governing the density.

A. Thermodynamic Integration

Ten independent simulation runs of 10^8 MC steps each, were performed (10^7 steps of equilibration) on simulation boxes containing 864 atoms at three densities: $\tilde{v}^2 = 0.1$, 0.6, and 1.0. The samples of $U + \mathbf{F}\cdot\Delta\mathbf{r}/2$ and U were collected for calculating the harmonically-mapped and the conventional averages of $(U^{\rm ah}/T^2)_0$. Then, one atom was removed from each simulation box in order to create a vacancy defect, and another independent set of simulations were conducted to calculate $(U^{\rm ah}/T^2)_1$. Uncertainties were measured based on block averages taken across ten independent simulations at each temperature and density. At lower temperatures, no diffusion events were observed in any of the ten runs, so HMA results could be used in all cases, while at the highest temperatures all runs exhibited a diffusion event and only conventional averages were used to evaluate $U^{\rm ah}$; between these limits a mix of the conventional and HMA results from the ten runs were averaged.

TI was used to obtain free energies only for systems with zero and one vacancy, respectively, so calculations of the vacancy concentration using these data employ the noninteracting-vacancy approximation described in Sec. II D.

B. Particle insertion

The MC simulations were performed with 864 lattice sites at twelve densities: $\tilde{v}^2 = 0.0$, 0.1, 0.2, 0.3, 0.4, 0.5, 0.6, 0.7, 0.8, 0.9, 1.0, and 1.1, from near-zero temperature to the respective melting temperatures. Displacement and insertion/deletion trials were attempted with approximately a 10:1 ratio (displacement:insertion/deletion). Simulations sampled 10^7 trials after 10^6 equilibration steps. Vacancy FE data were collected whenever an insertion or deletion move was attempted. Pressure was computed once every 864 steps. Uncertainty estimates are based on the variation of results obtained from ten independent simulations at each condition.

The particle-insertion calculations sample the grand-canonical ensemble, as described in Sec. III B. Hence, in these simulations we collect data for varying numbers of vacancies, and no noninteracting-vacancy approximation is invoked in analyzing the results to determine vacancy concentrations.

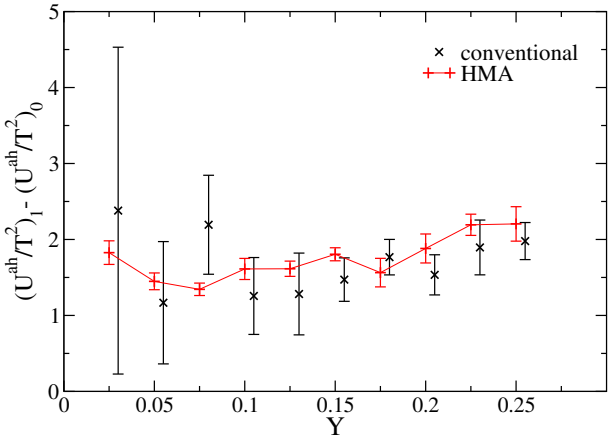

FIG. 2: Comparison of the precision obtained by using harmonically-mapped and conventional averaging methods, for the calculation of anharmonic energies of vacancy formation; the system of study is an LJ fcc crystal of density 1.0 (LJ units). Values from conventional averaging are shifted to the right by 0.005 for clarity. Lines join the HMA values as a guide to the eye.

The free energy A_0 for the vacancy-free system was evaluated by thermodynamic integration, as reported elsewhere [33].

V. RESULTS AND DISCUSSION

A. Vacancy Formation Free Energy

Figure 2 presents the temperature dependence of $(U^{\rm ah}/T^2)_1 - (U^{\rm ah}/T^2)_0$ for the isochore of density 1.0, from near-zero temperature up to its melting temperature; these results were obtained using HMA and conventional averaging methods. The size of the error bars associated with the two methods clearly illustrates the improved performance of HMA versus conventional averaging. The contrast is particularly striking at lower temperatures, where conventional averaging is unable to discern a difference that is statistically non-zero.

According to the TI technique (Eq. (26)), the area under this curve can be used to calculate the anharmonic vacancy formation FE. To this end, $(U^{\rm ah}/T^2)_1 - (U^{\rm ah}/T^2)_0$ versus temperature data sets for the three isochores were fit to straight lines (first-order polynomials), and the anharmonic vacancy formation free energies were calculated using the area under these fits. Thereafter, the contributions to vacancy formation from the lattice energy and the harmonic FE (Eqs. (24), (25)) were added, in order to calculate the total vacancy formation free energies.

Figure 3 presents the results of the vacancy formation free energies (ΔA_1), at the three isochores ($\tilde{v}^2$: 0.1, 0.6, and 1.0), obtained using the harmonic approximation, HMA, conventional TI, and particle insertion (PI) methods. At low temperatures (small Y), the harmonic ap-

proximation results are in agreement with the other three methods; however, at higher temperatures the results deviate significantly due to the presence of non-negligible anharmonic contributions. At all temperatures examined in this study, the results obtained by the other three FE methods overlap within the uncertainty limits (Supplementary Material). However, our motivation here is to compare the relative efficiency of these three methods. Accordingly, the relative difficulty in obtaining these results is examined in the next section.

Often the vacancy formation free energy is approximated by the vacancy energy alone, ignoring entropic contributions. Figure 3 shows that this is a poor approximation, and leads to considerable underestimation of the vacancy concentration. In the figure, the error incurred in $\beta\Delta A_1$ can be given as the slope of the line joining a plotted point at the condition of interest, to the $Y = 0$ intercept of its isochore. Inasmuch as the plotted isochores are nearly linear, we may take this simply as the slope of the isochore for the volume of interest. While the slopes vary a bit with $\tilde{v}^2$, all are about equal to -10. A shift in $\beta\Delta A_1$ of this magnitude corresponds to an underestimation of the vacancy concentration of $\exp(-10)$ (Eq. (22)), or more than four orders of magnitude.

Interestingly, with a classical treatment of the harmonic behavior, the intercept (i.e., the lattice energy) is approached with a non-zero slope, so this error is persists, unattenuated, even in the limit of low temperature, where one would expect the lattice-energy approximation to be valid. If instead using the (physically correct) non-classical treatment of the harmonic free energy, the approach to $T = 0$ is made with zero slope, but the intercept is not the lattice energy, as it also includes contributions from the quantum oscillator zero-point energy. This temperature-independent error in ΔA_1 leads to a divergent error in the vacancy concentration at low temperature.

Comparison of the quasiharmonic isochores with the full anharmonic behavior, we see that the quasiharmonic treatment begins to deviate noticeably from the true behavior at about half the melting temperature for each isochore. Further, the error in the quasiharmonic $\beta\Delta A_1$ at melting is about the same for all isochores, and equal to about 2. This corresponds to an underestimation of the vacancy concentration at melting by about a factor of 7.

These observations are consistent with recent studies that have emphasized the importance of entropic effects and anharmonic contributions to the vacancy thermodynamics [1, 20, 34–36].

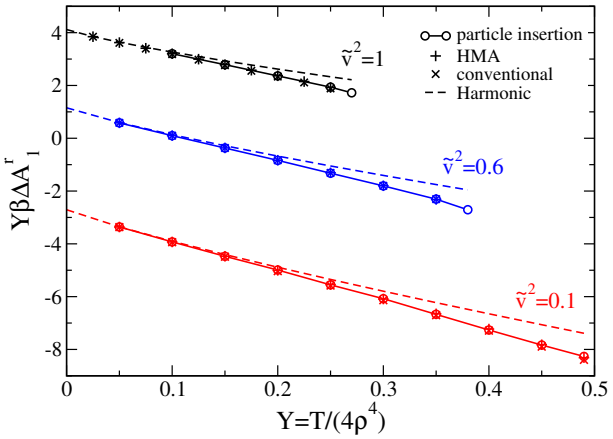

FIG. 3: Vacancy formation FE (ΔA_1) measurements at the three isochores ($\tilde{v}^2$: 0.1, 0.6, and 1.0) from zero temperature (where $\Delta A_1 = \Delta U^{\text{lat}}$) up to the respective melting temperatures; these results were obtained using four FE methods: (1) particle insertion; (2) HMA; (3) conventional TI; (4) harmonic approximation.

B. Difficulty Ratio

Figure 4 shows the relative performance of the three methods for calculating the vacancy formation free energies, in terms of the difficulty, $D \equiv t^{1/2}\sigma$, defined in terms of the CPU (central processing unit) time t required to obtain a stochastic average with uncertainty σ [37]. The plot compares the performance via the ratio of difficulties of the methods ($D^{\text{HMA}}/D^{\text{conv}}$ and $D^{\text{PI}}/D^{\text{conv}}$). The square of the difficulty ratio gives the ratio of CPU-times required by HMA/PI method and the conventional method to achieve a result of the same precision. The results indicate that both the HMA and particle insertion methods are much more efficient than the conventional method, as the difficulty ratios are less than 1 for all the conditions examined in this study. HMA is from 8 to 36 times faster than conventional averaging along the three isochores examined.

Also, the results demonstrate that for this LJ system the particle insertion method is much more computationally efficient than either conventional or the HMA TI methods — it gives results to the same precision 15 to 4500 times faster than conventional averaging. This is because the particle insertion method benefits from the biasing used to ensure that insertions were attempted at locations more likely to be accepted. Additionally, when applied to a single thermodynamic state, particle insertion requires only a single simulation for vacancy formation FE calculation, whereas the TI technique requires multiple simulations from near-zero temperature to the temperature of interest in order to integrate along a reversible thermodynamic path. Thus, TI approaches demand much higher CPU time for obtaining similar precision. However, the implementation of HMA is straightforward even for complex molecular systems like ice, acetic acid, clathrates, etc., where particle insertion becomes increasingly difficult. Hence, though particle insertion is highly efficient for simple systems, HMA would be a more effective approach for complicated structures where insertion is infeasible.

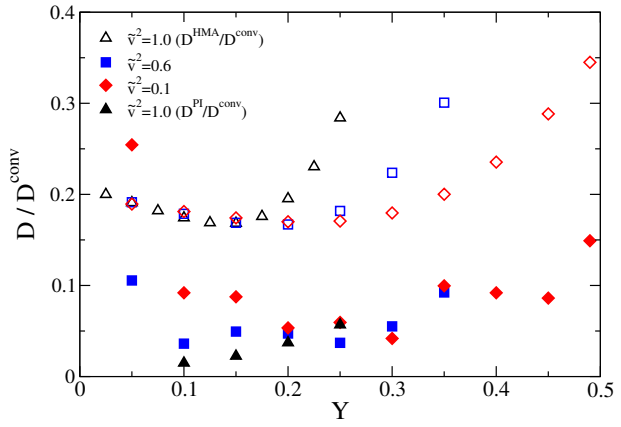

FIG. 4: Comparison of the difficulties of the three FE methods in obtaining vacancy formation free energies. The filled symbols indicate the difficulty ratio of particle insertion method with respect to conventional averaging method; the unfilled symbols indicate the difficulty ratio of HMA with respect to conventional averaging method.

C. Vacancy Concentration

Figure 5 presents the results for the vacancy concentration (ϕ) for a range of temperatures and densities. Part (a) represents the data in terms of the natural variables, allowing ϕ to be read easily from the graph for a given T and $\tilde{v}^2$. Part (b) shows the same data, but in terms of reduced variables $Y \ln \phi$ versus Y, again showing various isochores. With this representation we are able to present results for the entire range of stability of the crystal (including the $\tilde{v}^2 = 0$ soft-sphere limit), on a single graph.

Results for the three isochores where we have both TI and particle-insertion data are in statistical agreement. This is notable not only because it provides a demonstration of the correctness of the methods, but also because the TI results employ the noninteracting-vacancy approximation. The agreement shows that this is an excellent approximation for the LJ system at all conditions. Furthermore, calculations based on fixed M, Eq. (22), are indistinguishable from results obtained using the more rigorous framework that equilibrates the number of lattice sites.

Figure 5 (a) demonstrates that the vacancy concentration is highly sensitive to the changes in temperature as well as density. At a fixed density, it increases significantly with the increase in temperature; at a fixed temperature, it increases significantly with the increase in density. However, near the melting temperature, the vacancy concentration is almost the same for all the densities, ranging from 1×10^{-4} to 3×10^{-4}. Interestingly, the vacancy concentration of hard spheres at melting falls in this interval [38].

On the scale of Fig. 5 (b), the vacancy concentration varies regularly with $\tilde{v}^2$ at fixed Y. This plot also makes the noise in the data visible at large Y.

D. Solid Properties

We can combine an equation of state for the vacancy-free fcc crystal [33] with the free energy difference due to vacancies (Eq. (13)) to obtain an equation of state for the fcc crystal with vacancies. In Fig. 6, we present the effect of vacancies on the pressure as a function of Y for various densities. Each curve terminates at the melting point. In the limit of infinite density ($\tilde{v}^2 = 0$), the potential is purely repulsive and having vacancies lowers the pressure for all temperatures. As the density decreases, the interactions become more attractive until they act cohesively at $\tilde{v}^2 = 1$ and cause the pressure to increase upon allowing vacancies to form. We also present the approximation described in Ref. [5]:

$$\Delta P \approx \phi kT/\tilde{v}, \tag{37}$$

estimating the pressure change this way using our calculated values of ϕ. Equation (37) comes from a formulation based on noninteracting vacancies, which is a valid approximation here; however, it does not account for changes in the chemical potential due to vacancies, and this leads to the discrepancy seen in the figure.

In Figure 7, we plot the difference in fcc-liquid coexistence pressure with and without accounting for vacancies. The effect of vacancies is to lower the coexistence pressure. We also observe excellent agreement with the approximation given in Ref. [5]:

$$\beta \Delta P_{\rm coex} = -\frac{\phi}{v_{\rm l} - v_{\rm s}}. \tag{38}$$

The magnitude of the effect of vacancies is about half (and opposite in sign) of the finite-size effect accompanying the use of a vacancy-free 500-atom system instead of one extrapolated to the thermodynamic limit.

VI. CONCLUSION

The framework developed here for evaluating vacancy concentrations while equilibrating the number of lattice sites is little more complicated to apply than one that does not recognize the need for equilibration. Both approaches require free-energy differences for creation of one, two, etc. vacancies, while the proposed approach also requires evaluation of the ensemble-averaged pressure as a function of numbers of vacancies. This is not a significant complication, so on the one hand there should be no reason to perform vacancy-effect calculations that are in principle inaccurate because they do not equilibrate M. On the other hand, the effect of equilibrating M is completely negligible for the simple LJ model. Further, it appears to be a reasonable approximation to assume vacancies are noninteracting, and this introduces a significant simplification, in that only the FE difference between zero- and one-vacancy systems is needed. These outcomes (relating to M equilibration and noninteracting

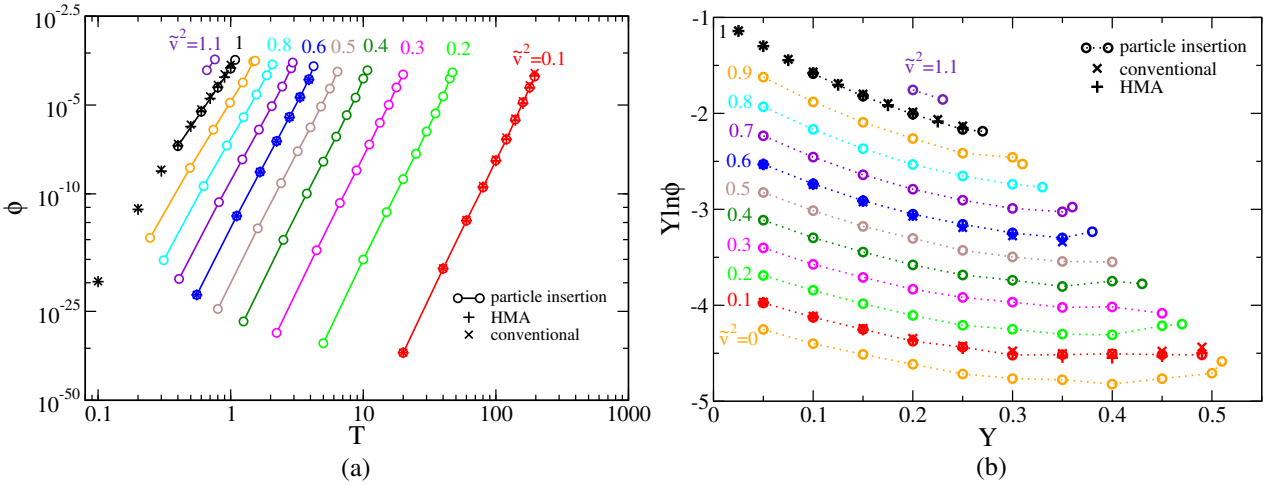

FIG. 5: Calculated vacancy concentrations across a range of states of the fcc LJ crystal, obtained by computing vacancy free energies via particle insertion and (for three of the isochores) conventional and HMA TI. (a) Vacancy concentration ϕ as a function of temperature T for several isochores, with $\tilde{v}^2$ as indicated. Note that ordinate is a "double-log" scale, such that the *exponents* of the values vary as on a logarithmic scale. Each isochore extends up to its respective melting temperature; (b) Same data as (a), but using scaled axes that permit all data to be presented. In both figures, uncertainties are smaller than or equal to (for points near melting) the symbol size for the particle-insertion and HMA results, and are about 3 times larger than the symbols for conventional TI near melting (not shown for clarity of figure).

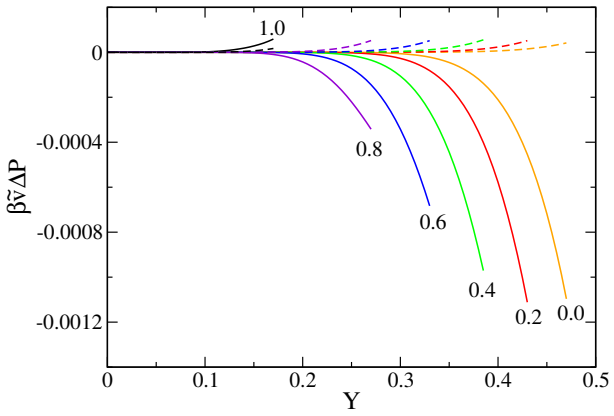

FIG. 6: Effect of vacancies on pressure (difference from no-vacancy value) as a function of Y for various values of $\tilde{v}^2$ (as labeled on each curve, increasing from right to left). Dashed lines are formula due to Pronk and Frenkel [5].

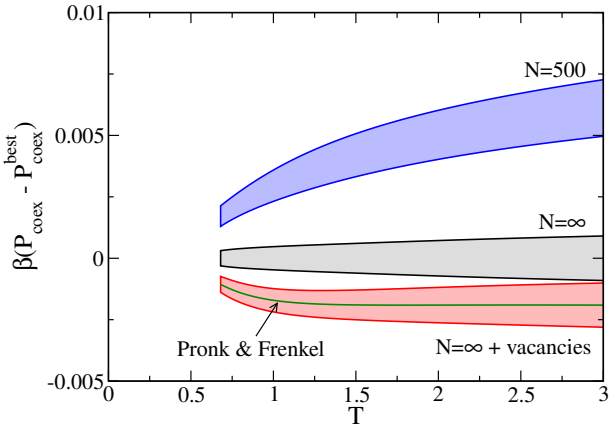

FIG. 7: Impact of finite-size effects (top curve) and vacancies (bottom curve) on the coexistence pressure. Each curve corresponds to a separate data set and the shading characterizes the uncertainty (68% confidence intervals). Each set is subtracted from the vacancy-free $N = \infty$ data. The estimate of the effect of vacancies as given by the formula of Pronk and Frenkel [5] is shown by the line, which is superimposed on our simulation data.

vacancies) may not apply in general, so for other systems it would be worthwhile to examine, for example, whether results change when using Eq. (21) instead of (22) and/or when a second interacting vacancy is considered.

For the convenience of the reader, we summarize here the key steps required to use the framework proposed here.

- Evaluate the change in free energy ΔA_n between systems having 0 versus n vacancies, using or thermodynamic integration in temperature for each n of interest, or grand-canonical averaging as described in Sec. III. If employing the noninteracting-vacancy approximation, only $n = 1$ is needed.

- Evaluate the ensemble-averaged pressure for each n, typically in the same simulations used to evaluate ΔA_n.

- Evaluate that zero-vacancy free energy, A_0 using an appropriate free-energy method (e.g., thermodynamic integration).

- Determine the value of λ that solves Eq. (5), where L is given by (2), $\bar{P}$ is given by (4), with p_n given

by (3).

- Using the so-determined value of λ, evaluate the vacancy concentration ϕ via Eq. (6).

- Alternatively, if using the noninteracting-vacancy approximation, solve for ϕ in Eq. (21). If ΔP_1 is unavailable, Eq. (22), which does not include the effect of equilibrating M, may be used.

Fluctuations in $\bar{P}$ are one of the primary sources of uncertainty within this approach unless P_0 is computed with mapped averaging. Since the MC simulations utilizing particule insertions did not use mapped averaging to compute the pressure, we replace P_0 with the pressure computed in separate simulations.

We have applied the framework to calculate the vacancy concentration and coexistence pressure of fcc LJ crystals at conditions that encompass the entire region of their stability. The vacancy formation free energies required in the treatment were obtained using three FE methods: (1) particle insertion in a grand canonical framework; (2) the recently developed HMA TI method, and (3) conventional-averaging TI. The framework is effective at calculating the vacancy concentrations using any of the three FE methods. Similarly, the effect of vacancies on the coexistence pressure calculated using our results is consistent with the predictions of Ref. [5]. Calculations based on the lattice energy alone, ignoring entropic contributions, underestimate the vacancy concentration by about four orders of magnitude at almost all conditions; ignoring only anharmonic contributions leads to an underestimate of the concentration by nearly one order of magnitude at melting.

We have also compared the computational efficiency of the three FE methods. Our results show that the conventional TI method is the least efficient method, and hence, HMA TI method is more desirable for anharmonic calculations of thermodynamic properties of crystalline systems. The particle insertion method is the most computationally efficient method out of the three methods; however, its implementation can be challenging for complex molecular systems. Thus, though particle insertion is highly efficient for simple systems, HMA may be more applicable approach for complicated structures where insertion is infeasible.

ACKNOWLEDGMENTS

This work was supported by the U.S. National Science Foundation, grants OAC-1739145, CBET-1510017, and CHE-1362572. Computational resources were provided by the Center for Computational Research (CCR), University at Buffalo.

APPENDIX

A. An illustrative model

We demonstrate the formalism outlined in Sec. II, presenting it here in the context of a simple tractable model that exhibits some of the thermodynamic anomalies that are introduced by failure to properly sample M. This is a noninteracting athermal cell model, in which each atom samples positions a cell, with available volume $V/M - v_{\rm cp}$; here $v_{\rm cp}$ is the value of V/M at the close-packed volume. We stipulate further that this available volume increases by a fraction f for each of the z atoms that neighbor a vacancy. There are $n \equiv M - N$ vacancies; we assume that configurations having adjacent vacancies are negligible. The canonical partition function for this model with fixed M is:

$$e^{-\beta A} = Q(V,N;M) = \binom{M}{N} \left(\frac{V}{M} - v_{\rm cp}\right)^N \xi^{M-N}, \tag{39a}$$

where we define $\xi \equiv (1+f)^z$. The binomial term in Eq. (39a) counts the ways to distribute the vacancies among the M lattice sites. The pressure and activity are:

$$\beta P(V,N;M) = -\left(\frac{\partial \beta A}{\partial V}\right)_M = \frac{N}{V - M v_{\rm cp}} \tag{39b}$$

$$\lambda(V,N;M) \equiv e^{\beta\mu} = \frac{Q(V,N;M)}{Q(V,N-1,M)} = \frac{1+M-N}{N\xi}\left(\frac{V}{M} - v_{\rm cp}\right). \tag{39c}$$

For a one-component system, a plot of μ versus P should be independent of volume. This is not the case for this model, however, as seen in Fig. 8 (a). This is one manifestation of the failure to sample M. Alternatively, we can examine adherence to the thermodynamic Euler equation, which states

$$A = -PV + N\mu. \tag{40}$$

This is shown in Fig. 8 (b), where we clearly see that the two sides of this equation differ — except at a single value of M. This point of intersection is the proper, equilibrium value of M for this N and V. The figure demonstrates this condition further, where we see that this value of M is also one that minimises the free energy A. Accordingly, we denote this as the equilibrium number of lattice sites, $M_{\rm eq}$, and we have

$$\left(\frac{\partial A}{\partial M}\right)_{T,V,N}\Bigg|_{M=M_{\rm eq}} = 0 \tag{41}$$

Note again in Fig. 8 (c) we show that the plot of μ versus P is properly invariant with V when both are evaluated for $M = M_{\rm eq}$.

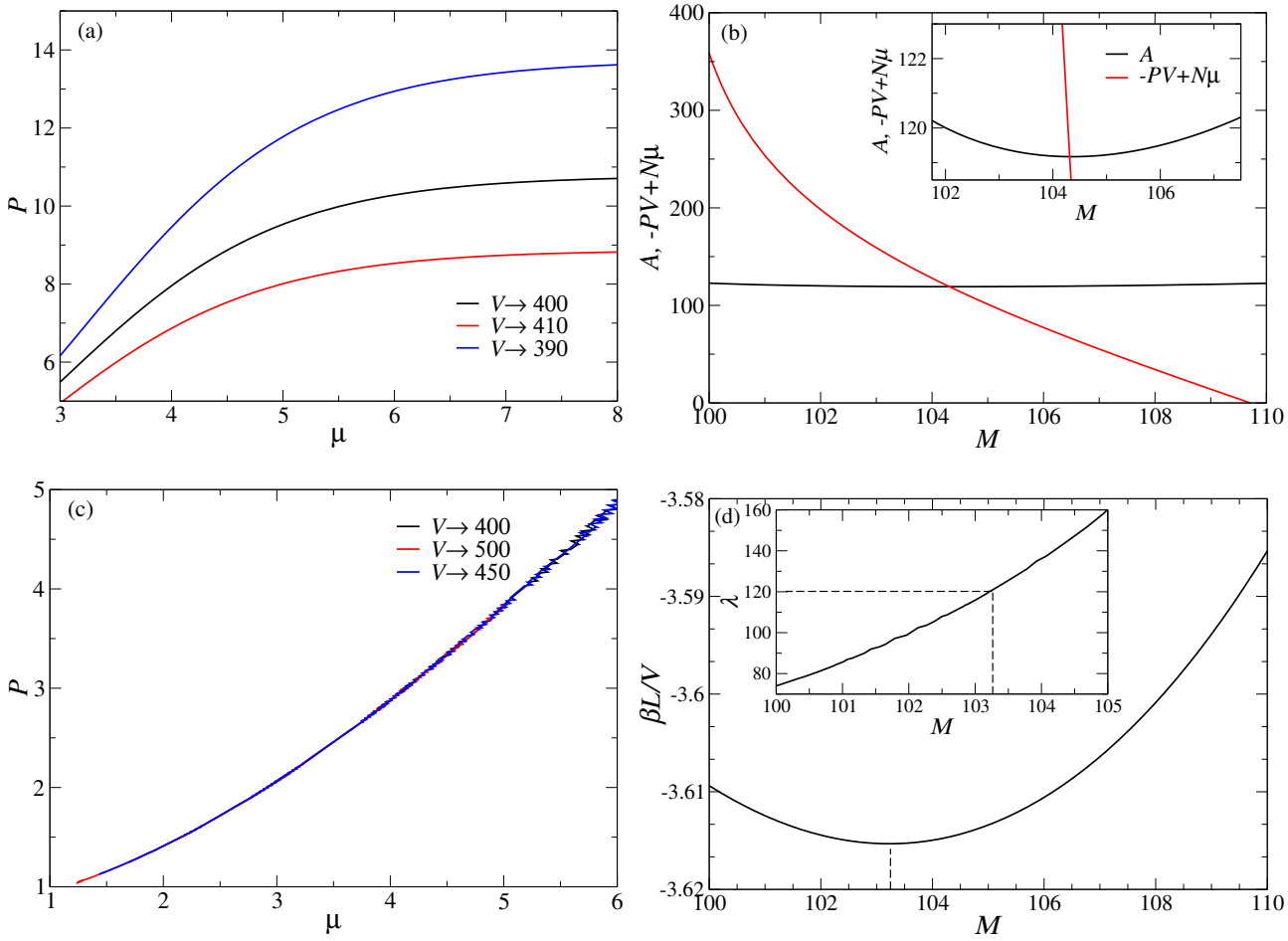

FIG. 8: Behavior of the simple cell model defined in Eq. (39) of Appendix A. All quantities are presented in arbitrary units. (a) Pressure versus chemical potential for several values of the total volume V (as indicated) and fixed number of lattice sites $M = 500$. (b) Demonstration of Euler relation for canonical ensemble, Eq. (40). Plotted are left- and right-hand sides of equation as a function of M; inset shows expanded view of point of intersection. (c) Same as (a), but for equilibrated rather than fixed M. (d) The current formalism successfully yields that λ ($\hat{\lambda} = 120$), for which any chosen M (say, $\hat{M} = 103.25$) minimises the grand-canonical free energy.

This model is by construction one with noninteracting vacancies (Sec. II D), so the grand potential L has the form given by Eq. (17), with

$$e^{-\beta\Delta A_1^{\rm r}} = \frac{\xi}{V/M - v_{\rm cp}} \tag{42}$$

Specifically, we may write

$$\beta L = -M \ln\left[\xi + \lambda\left(\frac{V}{M} - v_{\rm cp}\right)\right]. \tag{43a}$$

The pressure is:

$$\beta\bar{P} = \lambda\left[\xi + \lambda\left(\frac{V}{M} - v_{\rm cp}\right)\right]^{-1}. \tag{43b}$$

When Eq. (43) is used in Eq. (5), we obtain a formula for λ that depends only on the ratio $\tilde{v} \equiv V/M$ and not V or M individually:

$$\ln\left[\xi + \lambda\left(\tilde{v} - v_{\rm cp}\right)\right] = \lambda\tilde{v}\left[\xi + \lambda\left(\tilde{v} - v_{\rm cp}\right)\right]^{-1}; \tag{44}$$

solution of this equation defines $\lambda(\tilde{v})$. Accordingly, a parametric plot of $\bar{P}(\tilde{v})$ (from Eq. (43b)) versus $\lambda(\tilde{v})$ (from (44)) must be invariant with V, as required; this would not be the case if $\bar{P}$ versus λ were given by Eq. (43b) alone.

Having established the λ that yields M as the equilibrium number of lattice sites, the vacancy fraction can be determined from Eq. (6), which for this model may be summed to yield

$$\phi = \xi\left[\xi + \lambda\left(\frac{V}{M} - v_{\rm cp}\right)\right]^{-1} \tag{45}$$

Finally, to show that the approach based on determining λ via Eq. (5) is consistent with the view of $M_{\rm eq}$ minimizing the potential L for given λ, we present in Fig. 8

(d) a plot of $\beta L/V$ versus M for a fixed $V = 100$ and an arbitrarily selected value of λ, designated $\hat{\lambda} \equiv 120$. We also include on the figure a plot of $\lambda(V/M)$ given from Eq. (44), showing that the λ given this way coincides with $\hat{\lambda}$ where L versus M is a minimum. In other words, for a given M, Eq. (44) yields the λ for which the selected M minimises the grand-canonical free energy.
To obtain an expression for the intensive free energy a, we have $N \to \infty$ while $N/M = 1 - \phi$, yielding:

$$a(v;\phi) = -\frac{\phi}{1-\phi}\ln\xi + \ln(1-\phi) + \frac{\phi}{1-\phi}\ln\phi - \ln\left[(1-\phi)v - v_{\rm cp}\right] \tag{46}$$

Note that the equilibribum ϕ is given by (numerical) solution of $(\partial a/\partial\phi)_v = 0$. The pressure according to Eq. (8a) is

$$P = \frac{1-\phi}{(1-\phi)v - v_{\rm cp}}. \tag{47}$$

B. Justification of approach

The framework described in Sec. II allows us to determine the equilibrium λ corresponding to a specified M, for some choice of V and T. First, in this Appendix we show that in satisfying the Euler relation, Eq. (5), we minimise L with respect to M for given λ, T, and V. Then we show that neglect of fluctuations in M may be treated as a finite-size effect.

To differentiate with M, we consider a finite perturbation to scale up all of the system's extensive quantities by a factor $(1+\epsilon)$, such that the change in V and M are ϵV and ϵM, respectively. Given that the free energy L is extensive too, as a consequence its value will change by ϵL. If we subsequently perturb the volume back to its original value (at fixed M), then the total change in L for this process is

$$\Delta L = \epsilon L + \left(\frac{\partial L}{\partial V}\right)_{M,\lambda,T}(-\epsilon V). \tag{48}$$

Since the net change ΔL owes solely to the change in M, we can form the M derivative by dividing both sides by $\Delta M = \epsilon M$, yielding

$$M\left(\frac{\partial L}{\partial M}\right)_{V,\lambda,T} = L + \left(\frac{\partial L}{\partial V}\right)_{M,\lambda,T} V. \tag{49}$$

For the V derivative, we have

$$\begin{aligned}\left(\frac{\partial L}{\partial V}\right)_{M,\lambda,T} &= {\rm e}^{\beta L}\sum_n \left(\frac{\partial A_n}{\partial V}\right)_{M,V,T}\lambda^{M-n}{\rm e}^{-\beta A_n} \\ &= -{\rm e}^{\beta L}\sum_n P_n \lambda^{M-n}{\rm e}^{-\beta A_N} \\ &= -\bar{P}.\end{aligned} \tag{50}$$

So,

$$M\left(\frac{\partial L}{\partial M}\right)_{V,\lambda,T} = L - \bar{P}V \tag{51}$$

Hence, when Eq. (5) is satisfied, we have,

$$\left(\frac{\partial L}{\partial M}\right)_{V,\lambda,T} = 0, \tag{52}$$

which is what we set out to prove.

Now, we would like to consider the difference between this approach and one in which we include all M, for which the partition function is

$$\begin{aligned}\Xi &= \sum_M\sum_N \lambda^{M-n}{\rm e}^{-\beta A_n(M)} \\ &= \sum_M {\rm e}^{-\beta(L(M)-L_{M_{\rm eq}})}\Xi_{M_{\rm eq}} \\ &= \Xi(M_{\rm eq})\sum_M {\rm e}^{-\beta[L(M)-L(M_{\rm eq})]}\end{aligned} \tag{53}$$

We can approximate the free energy difference with a second-order series:

$$\beta[L(M) - L(M_{\rm eq})] \approx k(M - M_{\rm eq})^2 \tag{54a}$$

where

$$k \equiv \frac{\beta}{2}\left(\frac{\partial^2 L}{\partial M^2}\right)_{V,\lambda,T}. \tag{54b}$$

Then the sum in (54a) yields, for $kM_{\rm eq}^2 \gg 1$

$$\Xi = \left(\frac{\pi}{k}\right)^{1/2}\Xi(M_{\rm eq}) \tag{55}$$

To obtain the second derivative that defines k, we follow the same perturbation process outlines above, but include the second-order terms when scaling back the volume, thus:

$$\Delta L = \epsilon L + \left(\frac{\partial L}{\partial V}\right)_{M,\mu,T}(-\epsilon V) + \frac{1}{2}\left(\frac{\partial^2 L}{\partial V^2}\right)_{M,\mu,T}(\epsilon V)^2. \tag{56}$$

The first two terms cancel at equilibrium, as does $\partial L/\partial M$, leaving

$$\begin{aligned}\left(\frac{\partial^2 L}{\partial M^2}\right)_{V,\lambda,T} &= \tilde{v}^2\left(\frac{\partial^2 L}{\partial V^2}\right)_{M,\lambda,T} \\ &= -\tilde{v}^2\left(\frac{\partial \bar{P}}{\partial V}\right)_{M,\lambda,T}\end{aligned} \tag{57}$$

The free energy is then

$$\beta L = \beta L(M_{\rm eq}) + \frac{1}{2}\ln\left[-\frac{\beta\tilde{v}^2}{2\pi}\left(\frac{\partial\bar{P}}{\partial V}\right)_{M,\lambda,T}\right] \tag{58}$$

The argument to the logarithm is positive because thermodynamic stability requires that $\left(\partial \bar{P}/\partial V\right)_{M,\lambda,T} < 0$.

We see that the correction to $L(M_{\rm eq})$ to allow for fluctuations in M introduces terms of order $\ln M$. This becomes negligible in comparison to L (which is $\mathcal{O}(M)$) in the thermodynamic limit (where $M \to \infty$); hence it may be treated as another finite-size effect.

[1] C. Freysoldt, B. Grabowski, T. Hickel, J. Neugebauer, G. Kresse, A. Janotti, and C. G. Van de Walle, Rev. Mod. Phys. **86**, 253 (2014).
[2] J. C. Bourgoin, Radiat. Eff. **79**, 235 (1983).
[3] Y. Kraftmakher, Phys. Rep. **299**, 79 (1998).
[4] W. Swope and H. Andersen, Phys. Rev. A **46**, 4539 (1992).
[5] S. Pronk and D. Frenkel, J. Phys. Chem. B **105**, 6722 (2001).
[6] P. A. Monson and D. A. Kofke, Adv. Chem. Phys. **115**, 113 (2000).
[7] D. A. Kofke, Mol. Phys. **102**, 405 (2004).
[8] D. A. Kofke, Fluid Phase Equilib. **228**, 41 (2005).
[9] M. A. Tschopp, M. Horstemeyer, F. Gao, X. Sun, and M. Khaleel, Scr. Mater. **64**, 908 (2011).
[10] S. Chandra, M. K. Samal, V. M. Chavan, and R. J. Patel, AIP Conf. Proc. **1731**, 100001 (2016).
[11] A. V. Avdeeva, J. Phys.: Conf. Ser. **653**, 012028 (2015).
[12] R. LeSar, R. Najafabadi, and D. J. Srolovitz, Phys. Rev. Lett. **63**, 624 (1989).
[13] R. Najafabadi and D. J. Srolovitz, Phys. Rev. B **52**, 9229 (1995).
[14] L. Zhao, R. Najafabadi, and D. J. Srolovitz, Modell. Simul. Mater. Sci. Eng. **1**, 539 (1993).
[15] F. A. Johnson, Proc. R. Soc. London, Ser. A **310**, 79 (1969).
[16] M. T. Dove, *Introduction to Lattice Dynamics:* (Cambridge University Press, Cambridge, 1993).
[17] S. M. Foiles, Phys. Rev. B **49**, 14930 (1994).
[18] E. Smargiassi and P. A. Madden, Phys. Rev. B **51**, 117 (1995).
[19] H. Wen, P.-W. Ma, and C. Woo, J. Nucl. Mater. **440**, 428 (2013).
[20] B. Grabowski, L. Ismer, T. Hickel, and J. Neugebauer, Phys. Rev. B **79**, 134106 (2009).
[21] S. G. Moustafa, A. J. Schultz, and D. A. Kofke, Phys. Rev. E **92**, 043303 (2015).
[22] D. Frenkel and B. Smit, *Understanding Molecular Simulation*, 2nd ed. (Academic Press, Inc., Orlando, FL, USA, 2001).
[23] T. B. Tan, A. J. Schultz, and D. A. Kofke, J. Chem. Phys. **132**, 214103 (2010).
[24] M. A. van der Hoef, J. Chem. Phys. **113**, 8142 (2000).
[25] Annu. Rev. Mater. Res. **32**, 195 (2002).
[26] W. C. Swope and H. C. Andersen, J. Chem. Phys. **102**, 2851 (1995).
[27] K. S. Rane, S. Murali, and J. R. Errington, J. Chem. Theory Comput. **9**, 2552 (2013).
[28] A. J. Schultz and D. A. Kofke, J. Comput. Chem. **36**, 573 (2015).
[29] R. Agrawal and D. A. Kofke, Mol. Phys. **85**, 43 (1995).
[30] M. A. van der Hoef, J. Chem. Phys. **113** (2000).
[31] M. A. van der Hoef, J. Chem. Phys. **117**, 5092 (2002).
[32] E. A. Mastny and J. J. de Pablo, J. Chem. Phys. **127**, 104504 (2007).
[33] A. J. Schultz and D. A. Kofke, J. Chem. Phys. , submitted (2018).
[34] B. Cheng and M. Ceriotti, Phys. Rev. B **97**, 054102 (2018).
[35] A. Glensk, B. Grabowski, T. Hickel, and J. Neugebauer, Phys. Rev. X **4**, 011018 (2014).
[36] G. Lucas and R. Schäublin, Nucl. Instrum. Meth. B **267**, 3009 (2009), proceedings of the Ninth International Conference on Computer Simulation of Radiation Effects in Solids.
[37] A. J. Schultz and D. A. Kofke, J. Chem. Theory Comput. **10**, 5229 (2014).
[38] C. H. Bennett and B. J. Alder, J. Chem. Phys. **54**, 4796 (1971).